nature astronomy

Article

https://doi.org/10.1038/s41550-024-02253-4

A low-density ocean inside Titan inferred from Cassini data

In the format provided by the authors and unedited

nature astronomy

Article

https://doi.org/10.1038/s41550-024-02253-4

A low-density ocean inside Titan inferred from Cassini data

In the format provided by the authors and unedited

Contents

Supplementary figures **1** – **13**, Supplementary tables **1** – **4**, and References.

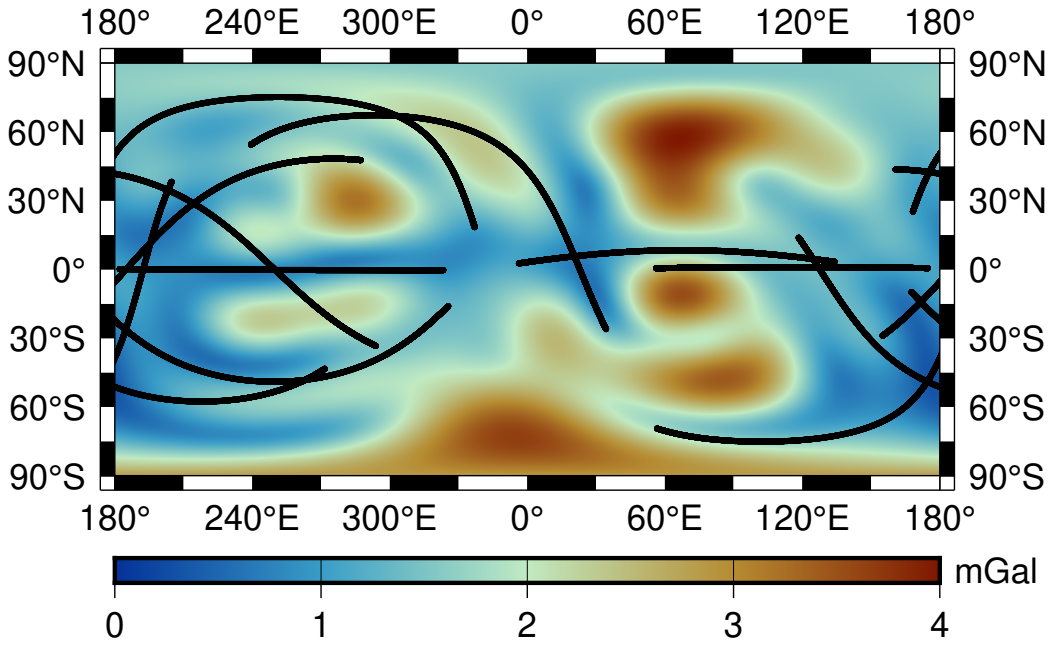

Supplementary Figure 1: Gravity formal errors for Titan from the full covariance matrix up to and including degree 5 of our solution. The ground tracks of the flybys are indicated in the same way as in Figure 1 of the main text.

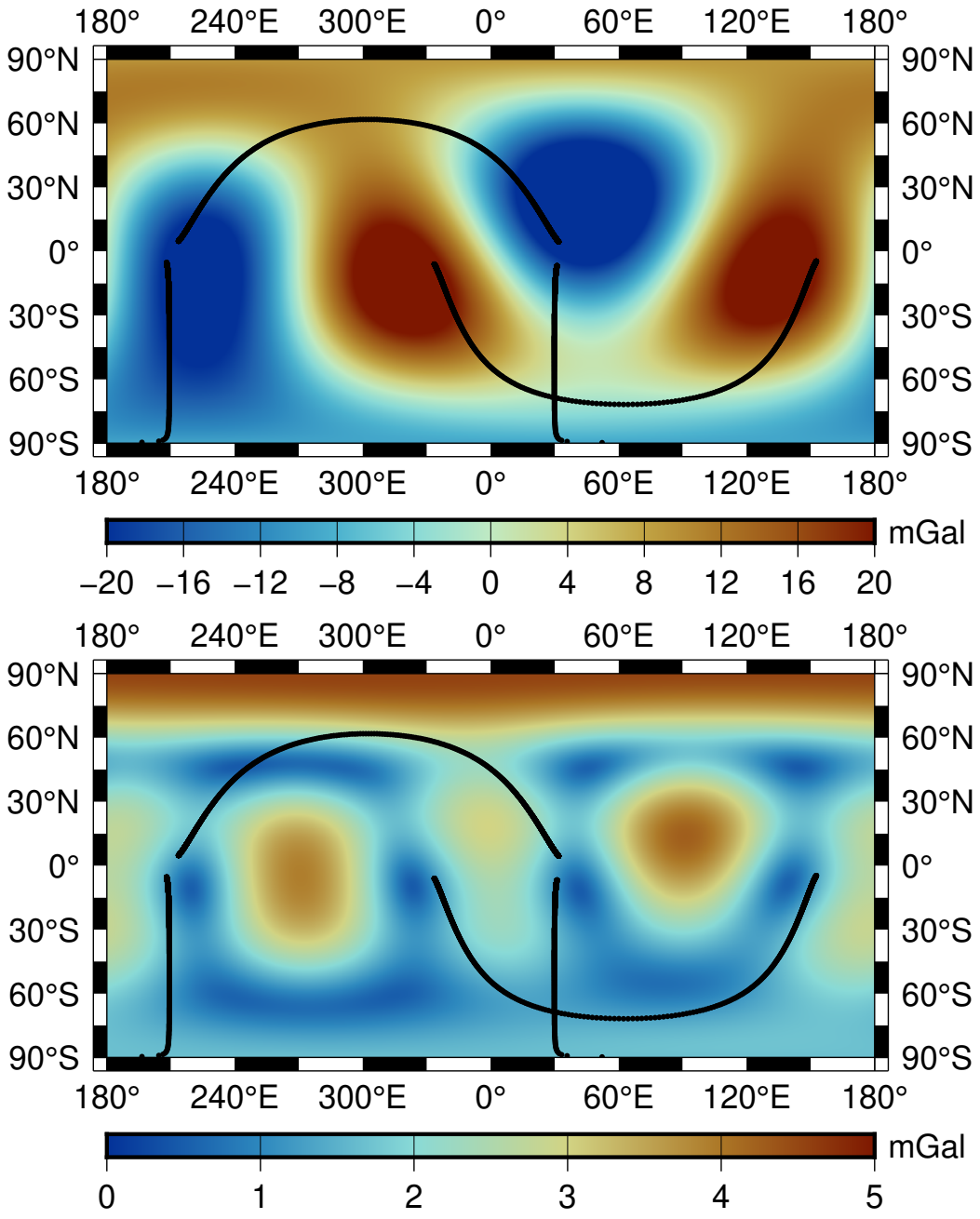

Supplementary Figure 2: Gravity expressed as radial accelerations for Enceladus (top) and formal errors from the full covariance matrix of our solution (bottom), both for the degree and order 2 field including the zonal term $\bar{C}_{3,0}$. The ground tracks of the flybys are indicated in black for altitudes less than 3,000 km. We set the coefficients $C_{2,0}$ and $C_{2,2}$ to zero for the gravity map.

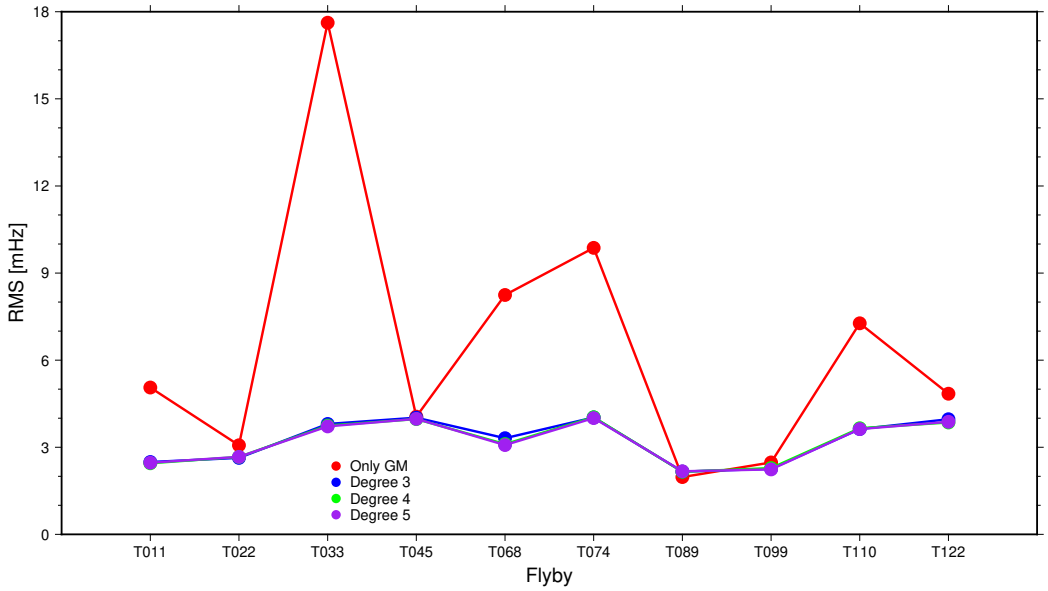

Supplementary Figure 3: Root-mean-square of Doppler data fit after gravity field determination for flybys for Titan for various expansions of the estimated gravity field. The entry labeled "Only GM" used the start value for GM with all other gravity terms set to zero. This shows that the fit did not change much when expanding from degree and order 3 up to 5.

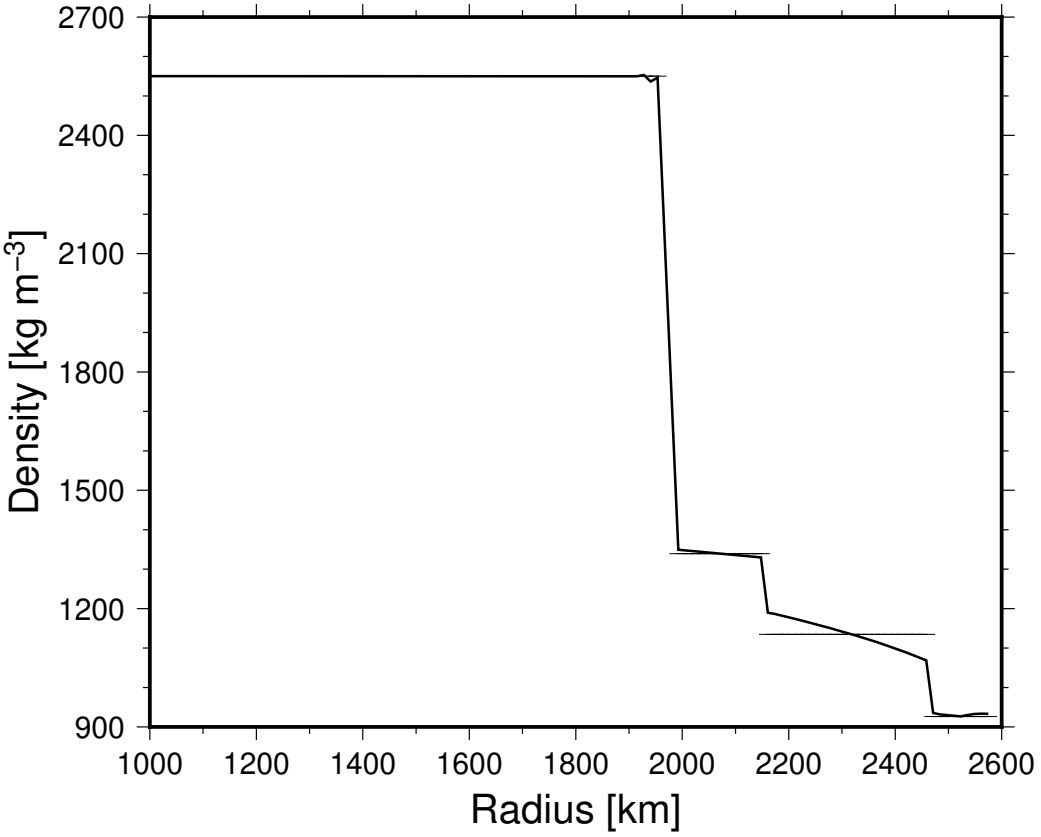

Supplementary Figure 4: Example of a density profile for the hydrosphere, using a pure water ocean with a temperature of 257 K at the base of the icy crust[31]. The core density is kept constant. We compared the tidal response of this density profile to that of a profile with constant densities, where the constant densities are the average densities in each layer of the hydrosphere. These constant densities are also indicated in the Figure.

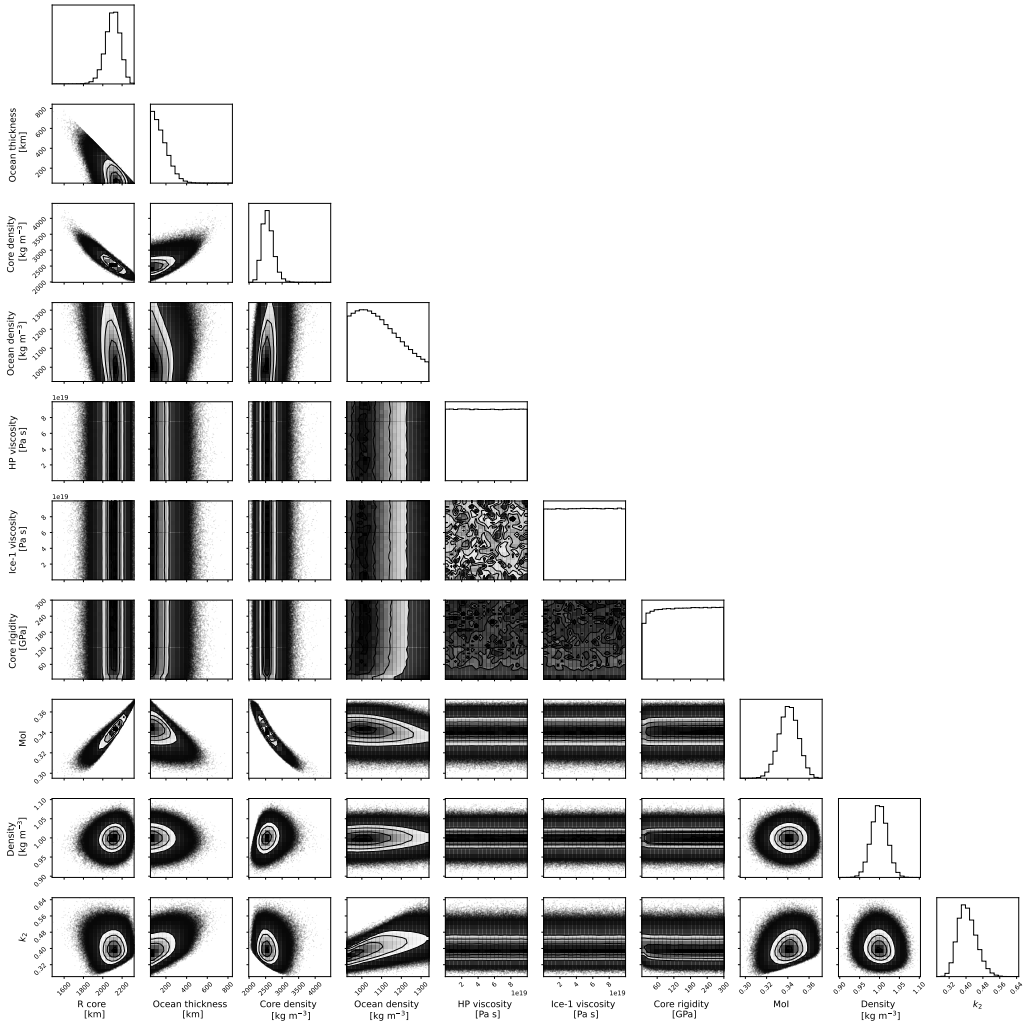

Supplementary Figure 5: Triangle plot of the distributions of the parameters and measurements for our Titan analysis using MCMC. Only a few parameters are well-determined as indicated by the distributions. The measurements are mapped well. This Figure is also available as a separate file. This figure was made with the Python package "corner" [45].

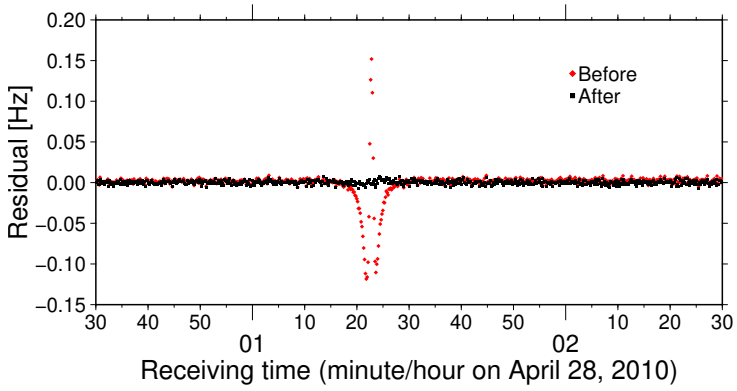

Supplementary Figure 6: Doppler residuals from Deep Space Network station DSS-55 for Enceladus flyby 009, before and after gravity field estimation. The closest approach signal is clearly visible in the pre-gravity determination residuals. The residuals after gravity estimation resemble measurement noise.

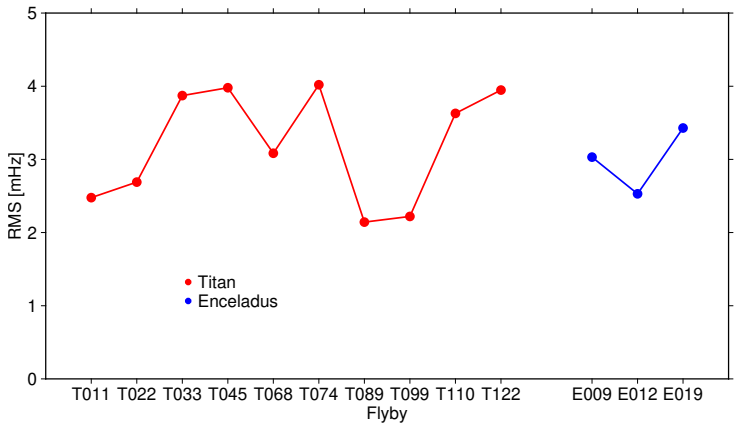

Supplementary Figure 7: Root-mean-square of Doppler data fit after gravity field determination for flybys for Titan (left/red) and Enceladus (right/blue).

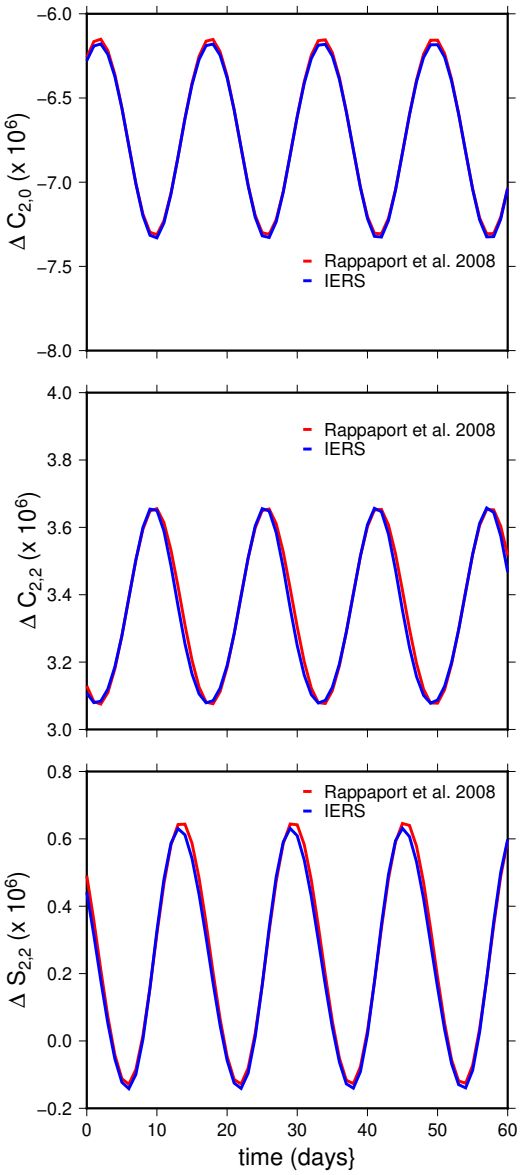

Supplementary Figure 8: Time-varying changes due to tides in the unnormalized degree 2 coefficients $C_{2,0}$ (top), $C_{2,2}$ (middle), and $S_{2,2}$ (bottom) using either a simplified potential[12] or the full expression[30], for 60 days in 2006.

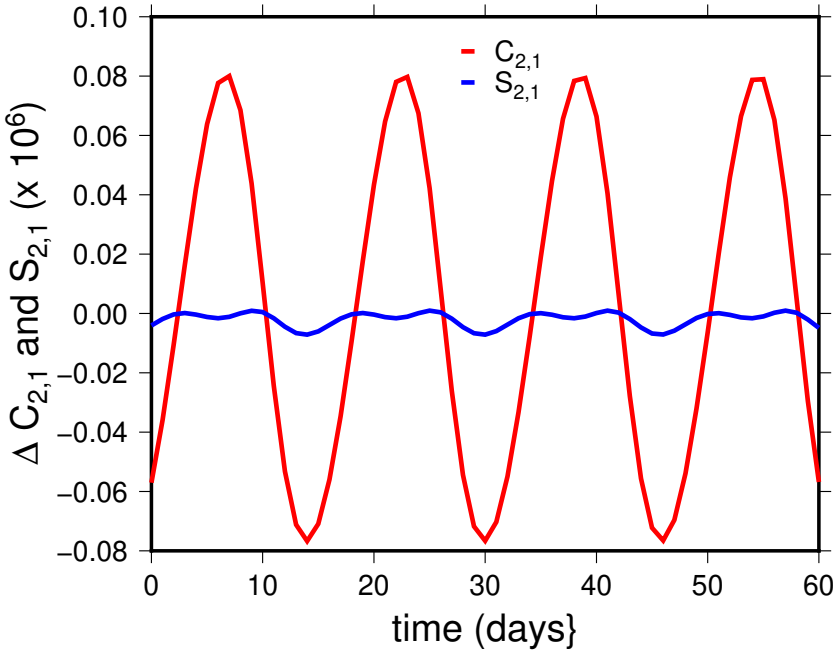

Supplementary Figure 9: Time-varying changes due to tides in the unnormalized degree 2 coefficients $C_{2,1}$ and $S_{2,1}$, from the full potential[30]. The variations are much smaller than those in the other degree 2 coefficients.

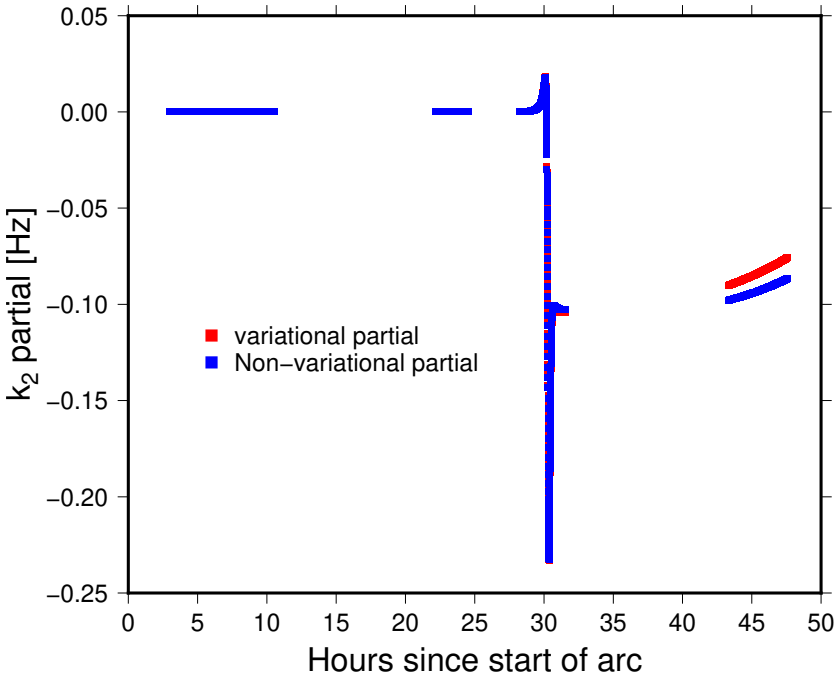

Supplementary Figure 10: Partials of Doppler data for Cassini flyby T022 with respect to k_2, directly computed using the full variational approach, or using the non-variational approach from eq. (12). We used the full IERS expressions, not the simplified potential[12], in order to have the exact same partials $\partial\nu_{2,m}/\partial k_2$.

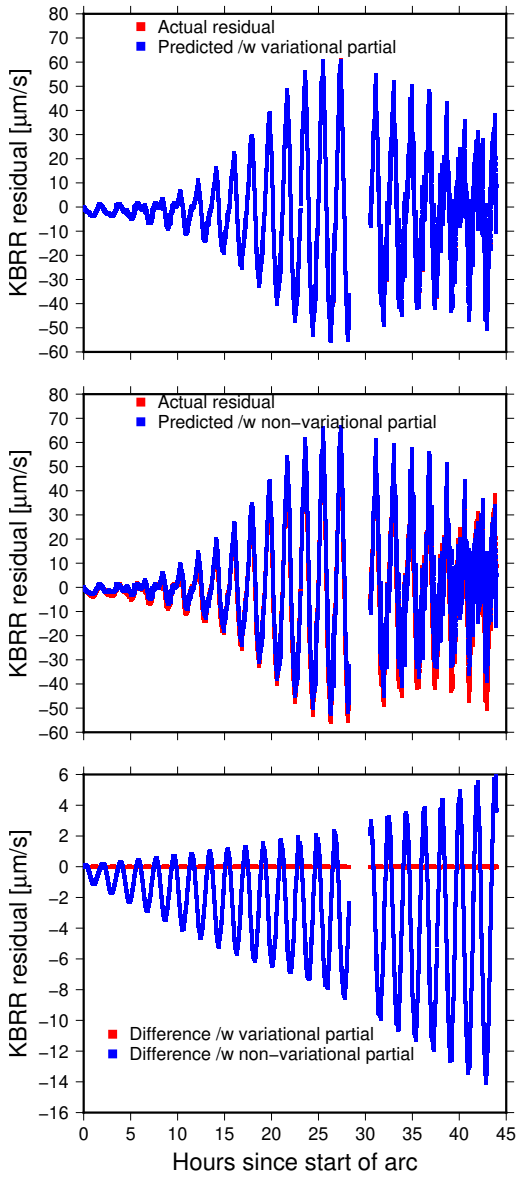

Supplementary Figure 11: Comparison of residual changes and those predicted from the partials, following eq. (11), for an arc for GRAIL Ka-Band Range-Rate (KBRR) data in April, 2012. We compare actual differenced residuals with the change in measurements as predicted by the partials for the case using the full variational approach (top) and for the case with the non-variational approach (middle). The difference between predicted and actual residual changes for both cases are shown in the bottom plot.

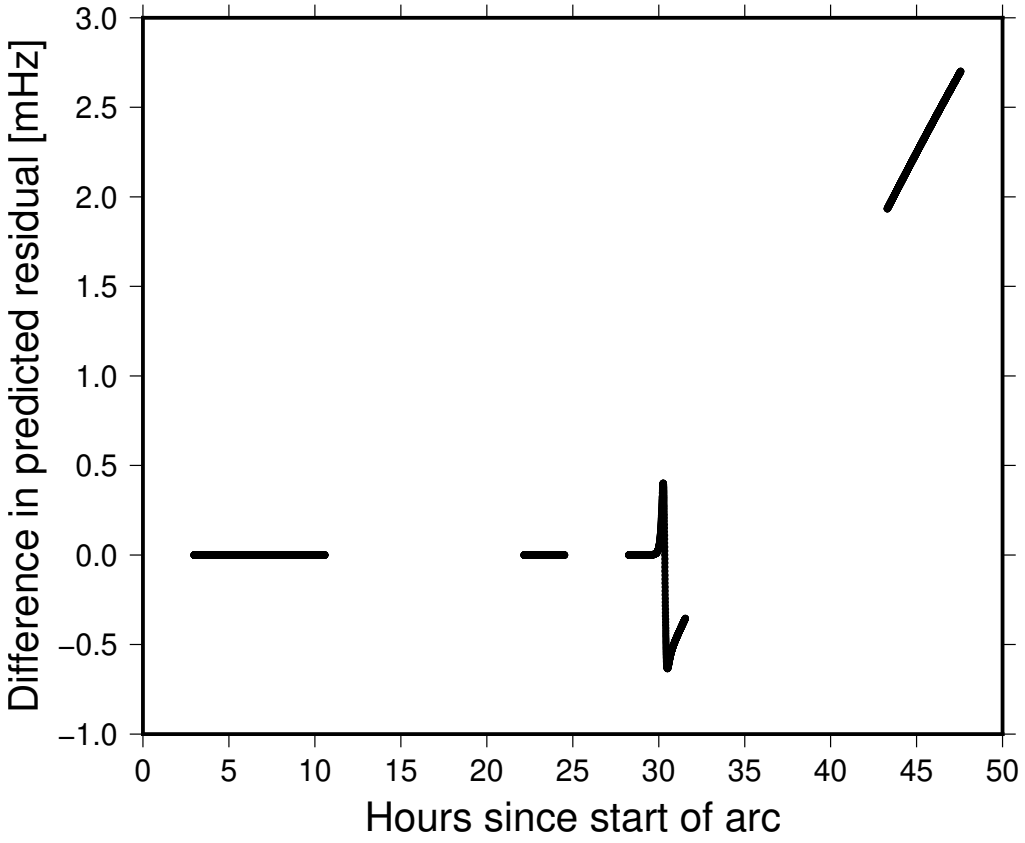

Supplementary Figure 12: Differences in residuals between those predicted by the variational partials (eq. 17) and those predicted by the non-variational partials (eq. 12) for Cassini flyby T022, using a Δk_2 of 0.25. These are constructed using the partials shown in Supplementary Figure **10**.

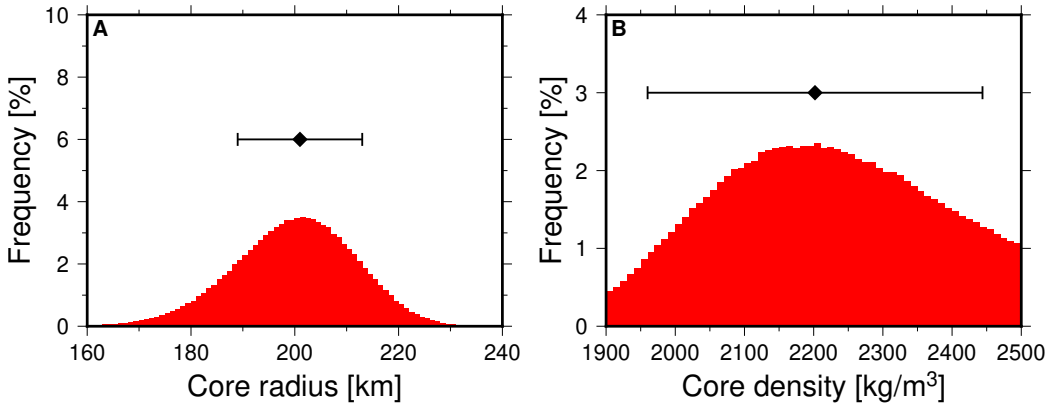

Supplementary Figure 13: A posteriori distributions (including the central value ± 1 standard deviation) of the core radius (left) and core density (right) for Enceladus as results from our Monte Carlo analysis to match the moment of inertia and bulk density. We evaluated 100,000 models using 40 chains.

Supplementary Table 1: Estimated gravity field coefficients for Enceladus and Titan. All spherical harmonic coefficients are unnormalized and their values are multiplied by 10^6. The moment of inertia factor $C/(MR^2)$ is computed from the Darwin-Radau relationship (see text). For Titan, the permanent tide contribution from k_2 is included in the degree two coefficients, and they are thus "zero tide" coefficients. This is also the case by definition for Enceladus since we do not model or estimate k_2 for that moon. Previous solutions for Enceladus[20] and Titan[3] are also included for comparison.

Enceladus	This work	Previous		This work	Previous
GM [km^3/s^2]	7.2107 ± 0.00007	7.2096 ± 0.0067			
J_2	5406.8 ± 175.5	5435.2 ± 34.9			
$C_{2,1}$	-170.9 ± 26.9	9.2 ± 11.6	$S_{2,1}$	-134.8 ± 57.1	39.8 ± 22.4
$C_{2,2}$	1638.1 ± 92.3	1549.8 ± 15.6	$S_{2,2}$	-237.8 ± 14.8	22.6 ± 7.4
J_3	-202.2 ± 116.9	-115.3 ± 22.9			
$J_2/C_{2,2}$	3.30 ± 0.27	3.51 ± 0.05			
$C/(MR^2)$	0.345 ± 0.01	0.335			
Titan					
GM [km^3/s^2]	8978.1269 ± 0.0008	8978.1383 ± 0.0003			
k_2	0.375 ± 0.06	0.616 ± 0.067			
J_2	36.256 ± 3.108	33.089 ± 0.609			
$C_{2,1}$	-0.738 ± 0.261	0.513 ± 0.215	$S_{2,1}$	-1.082 ± 0.625	0.612 ± 0.359
$C_{2,2}$	11.263 ± 1.285	10.385 ± 0.084	$S_{2,2}$	0.515 ± 0.143	-0.064 ± 0.066
J_3	0.628 ± 1.199	-0.179 ± 0.720			
$C_{3,1}$	1.045 ± 0.346	1.481 ± 0.254	$S_{3,1}$	-3.363 ± 0.705	0.811 ± 0.402
$C_{3,2}$	0.720 ± 0.322	0.183 ± 0.153	$S_{3,2}$	-0.337 ± 0.216	-0.027 ± 0.099
$C_{3,3}$	-0.113 ± 0.031	-0.222 ± 0.017	$S_{3,3}$	-0.099 ± 0.030	-0.226 ± 0.019
J_4	-3.074 ± 2.640	-1.077 ± 1.844			
$C_{4,1}$	-0.285 ± 0.492	-0.842 ± 0.299	$S_{4,1}$	-3.868 ± 1.053	0.191 ± 0.717
$C_{4,2}$	1.132 ± 0.202	0.183 ± 0.107	$S_{4,2}$	-0.206 ± 0.157	0.198 ± 0.106
$C_{4,3}$	0.031 ± 0.059	-0.012 ± 0.039	$S_{4,3}$	-0.046 ± 0.051	-0.062 ± 0.033
$C_{4,4}$	-0.003 ± 0.005	-0.014 ± 0.003	$S_{4,4}$	0.002 ± 0.005	-0.012 ± 0.004
J_5	-4.762 ± 3.270	1.118 ± 2.022			
$C_{5,1}$	0.340 ± 0.535	0.361 ± 0.406	$S_{5,1}$	-1.587 ± 0.830	0.267 ± 0.604
$C_{5,2}$	0.347 ± 0.184	-0.097 ± 0.118	$S_{5,2}$	-0.159 ± 0.156	0.044 ± 0.094
$C_{5,3}$	0.061 ± 0.030	-0.016 ± 0.019	$S_{5,3}$	0.067 ± 0.019	-0.004 ± 0.012
$C_{5,4}$	0.003 ± 0.006	0.007 ± 0.004	$S_{5,4}$	-0.019 ± 0.007	-0.002 ± 0.004
$C_{5,5}$	-0.001 ± 0.001	0.000 ± 0.001	$S_{5,5}$	0.000 ± 0.001	0.000 ± 0.001
$J_2/C_{2,2}$	3.21 ± 0.72	3.186 ± 0.077			
$C/(MR^2)$	0.348 ± 0.03	0.341			

Supplementary Table 2: Flyby altitude, date (yyyy-mm-dd), Titan's mean anomaly (not indicated for Enceladus flybys), VCE weight factor, and final data weight. A weight factor larger than one means that the data are up-weighted. C/A indicates closest approach.

Flyby	C/A altitude [km]	C/A date and time (UTC)	Mean anomaly [degree]	VCE factor	Data weight [mHz]
T011	1812	2006-02-27 08:25	173	186	2.05
T022	1297	2006-12-28 10:05	197	118	2.58
T033	1933	2007-06-29 17:00	15	84	3.06
T045	1614	2008-07-31 02:13	346	50	3.96
T068	1398	2010-05-20 03:24	81	136	2.40
T074	3651	2011-02-18 16:04	159	50	3.96
T089	1978	2013-02-17 01:56	65	182	2.08
T099	1500	2014-03-06 16:27	63	164	2.19
T110	2274	2015-03-16 14:30	248	60	3.61
T122	1698	2016-08-10 08:31	304	53	3.85
E009	97	2010-04-28 00:11	-	86	3.02
E012	43	2010-11-30 11:54	-	125	2.50
E019	70	2012-05-02 09:31	-	99	2.81

Supplementary Table 3: Results for k_2 from Cassini data for various cases of the k_2 partials. The formal errors are one sigma.

Case	Solution
fully variational partials	0.2835 ± 0.13
fully variational partials; periodic terms only	0.277 ± 0.13
fully variation partials; periodic, $S_{2,2}$ corrupted	0.345 ± 0.15
non-variational partial; IERS[30]	0.4527 ± 0.10
non-variational partial; Rappaport et al. (2008)[12]	0.366 ± 0.10
non-variational partial; Rappaport et al. (2008)[12], $S_{2,2}$ error	0.6736 ± 0.10

Supplementary Table 4: Parameters for the modeling of Titan's interior (based on earlier work[17]).

Parameter	Value or range
Core radius	> 0 km
High-pressure ice thickness	150 km
Ocean thickness	> 50 km
High-pressure ice density	1340 kg/m^3
Icy crust density	925 kg/m^3
Ocean density	925 kg/m^3 – 1340 kg/m^3
Core viscosity	10^{30} Pa s
High-pressure ice viscosity	10^{15} – 10^{20} Pa s
Ocean viscosity	25 kPa s
Icy crust viscosity	10^{13} – 10^{20} Pa s
Core unrelaxed rigidity	5 – 300 GPa
High-pressure ice unrelaxed rigidity	10 GPa
Ocean unrelaxed rigidity	10^{-30} GPa
Icy crust unrelaxed rigidity	3 GPa
Core bulk modulus	200 GPa
High-pressure ice bulk modulus	20 GPa
Ocean bulk modulus	2.5 GPa
Icy crust bulk modulus	10 GPa

References

[1] Iess, L. *et al.* Gravity Field, Shape, and Moment of Inertia of Titan. *Science* **327**, 1367–1369 (2010). Doi:10.1126/science.1182583.

[2] Tortora, P. *et al.* Rhea gravity field and interior modeling from Cassini data analysis. *Icarus* **264**, 264–273 (2016).

[3] Durante, D., Hemingway, D. J., Racioppa, P., Iess, L. & Stevenson, D. J. Titan's gravity field and interior structure after Cassini. *Icarus* **326**, 123–132 (2019).

[4] Zannoni, M., Hemingway, D., Gomez Casajus, L. & Tortora, P. The gravity field and interior structure of Dione. *Icarus* **345**, 113713 (2020).

[5] Iess, L. *et al.* Measurement and implications of Saturn's gravity field and ring mass. *Science* **364**, aat2965 (2019).

[6] Iess, L. *et al.* The Tides of Titan. *Science* **337**, 457–459 (2012). Doi:10.1126/science.1219631.

[7] Lunine, J. I. & Stevenson, D. J. Clathrate and ammonia hydrates at high pressure: Application to the origin of methane on Titan. *Icarus* **70**, 61–77 (1987).

[8] Grasset, O. & Sotin, C. The Cooling Rate of a Liquid Shell in Titan's Interior. *Icarus* **123**, 101–112 (1996).

[9] Grasset, O., Sotin, C. & Deschamps, F. On the internal structure and dynamics of Titan. *Planet. Sp. Sci.* **48**, 617–636 (2000).

[10] Sohl, F., Hussmann, H., Schwentker, B., Spohn, T. & Lorenz, R. D. Interior structure models and tidal Love numbers of Titan. *J. Geophys. Res.: Planets* **108**, 5130 (2003).

[11] Rappaport, N., Bertotti, B., Giampieri, G. & Anderson, J. D. Doppler Measurements of the Quadrupole Moments of Titan. *Icarus* **126**, 313–323 (1997).

[12] Rappaport, N. J. *et al.* Can Cassini detect a subsurface ocean in Titan from gravity measurements? *Icarus* **194**, 711–720 (2008).

[13] Sohl, F. *et al.* Structural and tidal models of Titan and inferences on cryovolcanism. *J. Geophys. Res.: Planets* **119**, 1013–1036 (2014).

[14] Sotin, C., Kalousová, K. & Tobie, G. Titan's Interior Structure and Dynamics After the Cassini-Huygens Mission. *Annu. Rev. Earth Planet. Sci.* **49** (2021).

[15] Stiles, B. W. *et al.* Determining Titan's Spin State from Cassini RADAR Images. *Astron. J.* **135**, 1669–1680 (2008). Doi:10.1088/0004-6256/135/5/1669.

[16] Zebker, H. A. *et al.* Size and Shape of Saturn's Moon Titan. *Science* **324**, 921 (2009).

[17] Mitri, G. *et al.* Shape, topography, gravity anomalies and tidal deformation of Titan. *Icarus* **236**, 169–177 (2014). Doi:10.1016/j.icarus.2014.03.018.

[18] Baland, R.-M., Tobie, G., Lefèvre, A. & Van Hoolst, T. Titan's internal structure inferred from its gravity field, shape, and rotation state. *Icarus* **237**, 29–41 (2014).

[19] Beuthe, M. Tidal Love numbers of membrane worlds: Europa, Titan, and Co. *Icarus* **258**, 239–266 (2015). Doi:10.1016/j.icarus.2015.06.008.

[20] Iess, L. *et al.* The Gravity Field and Interior Structure of Enceladus. *Science* **344**, 78–80 (2014). Doi:10.1126/science.1250551.

[21] Murray, C. & Dermott, S. *Solar System Dynamics* (Cambridge University Press, New York, USA, 1999).

[22] Meriggiola, R., Iess, L., Stiles, B. W., Lunine, J. I. & Mitri, G. The rotational dynamics of Titan from Cassini RADAR images. *Icarus* **275**, 183–192 (2016).

[23] Fortes, A. D. Titan's internal structure and the evolutionary consequences. *Planet. Sp. Sci.* **60**, 10–17 (2012). Doi:10.1016/j.pss.2011.04.010.

[24] Gao, P. & Stevenson, D. J. Nonhydrostatic effects and the determination of icy satellites' moment of inertia. *Icarus* **226**, 1185–1191 (2013). Doi:10.1016/j.icarus.2013.07.034.

[25] Coyette, A., Baland, R.-M. & Van Hoolst, T. Variations in rotation rate and polar motion of a non-hydrostatic Titan. *Icarus* **307**, 83–105 (2018).

[26] Zharkov, V. N., Leontjev, V. V. & Kozenko, V. A. Models, figures, and gravitational moments of the Galilean satellites of Jupiter and icy satellites of Saturn. *Icarus* **61**, 92–100 (1985).

[27] Asmar, S. W., Armstrong, J. W., Iess, L. & Tortora, P. Spacecraft Doppler tracking: Noise budget and accuracy achievable in precision radio science observations. *Radio Sci.* **40**, n/a–n/a (2005).

[28] Ermakov, A. I., Park, R. S. & Bills, B. G. Power Laws of Topography and Gravity Spectra of the Solar System Bodies. *J. Geophys. Res.: Planets* **123**, 2038–2064 (2018).

[29] Eanes, R., Schutz, B. & Tapley, B. Earth and ocean tide effects on Lageos and Starlette. *Proc. Ninth Int. Symp. Earth Tides* 239–249 (1983).

[30] McCarthy, D. D. & Petit, G. IERS Conventions (2003). *IERS Technical Note* **32** (2004).

[31] Vance, S. D. *et al.* Geophysical Investigations of Habitability in Ice-Covered Ocean Worlds. *J. Geophys. Res.: Planets* **123**, 180–205 (2018).

[32] Foreman-Mackey, D., Hogg, D. W., Lang, D. & Goodman, J. emcee: The MCMC Hammer. *Publ. Astron. Soc. Pac.* **125**, 306 (2013).

[33] Pavlis, D. E. & Nicholas, J. B. GEODYN II system description (vols. 1-5). contractor report, SGT Inc., Greenbelt, MD (2017). `https://earth.gsfc.nasa.gov/geo/data/geodyn-documentation`.

[34] Bertotti, B., Iess, L. & Tortora, P. A test of general relativity using radio links with the Cassini spacecraft. *Nature* **425**, 374–376 (2003).

[35] Archinal, B. A. *et al.* Report of the IAU Working Group on Cartographic Coordinates and Rotational Elements: 2015. *Celest. Mech. Dyn. Astron.* **130**, 22 (2018).

[36] Bellerose, J., Roth, D. & Criddle, K. The Cassini Mission: Reconstructing Thirteen Years of the Most Complex Gravity-Assist Trajectory

Flown to Date. *2018 SpaceOps Conf.* (American Institute of Aeronautics and Astronautics, Marseille, France, 2018). https://arc.aiaa.org/doi/10.2514/6.2018-2646.

[37] Barbaglio, F., Armstrong, J. W. & Iess, L. Precise Doppler Measurements for Navigation and Planetary Geodesy Using Low Gain Antennas: Test Results from Cassini. *Proc. 23rd Int. Symp. Sp. Flight Dyn.* (Pasadena, California, USA, 2012). https://issfd.org/ISSFD_2012/ISSFD23_OD1_4.pdf.

[38] Montenbruck, O. & Gill, E. *Satellite Orbits* (Springer-Verlag, Berlin, 2000).

[39] Tapley, B., Schutz, B. & Born, G. *Statistical Orbit Determination* (Elsevier Academic Press, Burlington, MA., USA, 2004).

[40] Kusche, J. Noise variance estimation and optimal weight determination for GOCE gravity recovery. *Adv. Geosci.* **1**, 81–85 (2003). Doi:10.5194/adgeo-1-81-2003.

[41] Běhounková, M., Souček, O., Hron, J. & Čadek, O. Plume Activity and Tidal Deformation on Enceladus Influenced by Faults and Variable Ice Shell Thickness. *Astrobiology* **17**, 941–954 (2017).

[42] Hemingway, D. J. & Mittal, T. Enceladus's ice shell structure as a window on internal heat production. *Icarus* **332**, 111–131 (2019).

[43] Renaud, J. P. TidalPy (0.4.1) (2023). https://zenodo.org/record/7017560.

[44] Styczinski, M. J., Vance, S. D. & Melwani Daswani, M. Planetprofile: Self-consistent interior structure modeling for ocean worlds and rocky dwarf planets in python. *Earth Space Sci.* **10**, e2022EA002748 (2023). https://agupubs.onlinelibrary.wiley.com/doi/abs/10.1029/2022EA002748. E2022EA002748 2022EA002748.

[45] Foreman-Mackey, D. corner.py: Scatterplot matrices in python. *J. Open Source Softw.* **1**, 24 (2016). https://doi.org/10.21105/joss.00024.

[46] Wessel, P., Smith, W. H. F., Scharroo, R., Luis, J. & Wobbe, F. Generic Mapping Tools: Improved Version Released. *EOS, Transactions American Geophysical Union* **94**, 409–410 (2013).

[47] Kaula, W. M. *Theory of Satellite Geodesy, applications of satellites to Geodesy* (Blaisdell Publishing Company, Waltham, MA., USA, 1966).